Ballistic Hall Photo-Voltammetry of Magnetic Resonance in Individual Nanomagnets

Alain Nogaret,[1,*] Maksym Stebliy,[2] Jean-Claude Portal,[3] Harvey E. Beere,[4] and David A. Ritchie[4]

[1]*Department of Physics, University of Bath, Bath BA2 7AY, UK*
[2]*School of Natural Sciences, Far Eastern Federal University, Vladivostok, 690091, Russia*
[3]*High Magnetic Field Laboratory, Centre National de la Recherche Scientifique, 25 Avenue des Martyrs, Grenoble 38042, France*
[4]*Cavendish Laboratory, J.J. Thomson Avenue, Cambridge CB3 0HE, UK*

We report on ballistic Hall photo-voltammetry as a contactless probe of localized spin excitations. Spins resonating in the near-field of a two-dimensional electron system are shown to induce a long range electromotive force which we calculate. We use this coupling mechanism to detect the spin wave eigenmodes of a single ferromagnet of sub-100nm size. The high sensitivity of this detection technique, 380 spins/$\sqrt{Hz}$, and its non-invasiveness present advantages for probing magnetization dynamics and spin transport.

Electrically detected spin resonance is a pivotal technique for probing the spin excitations of nano-sized ferromagnets [1–8] which underpin the coding of information in magnonic crystals [9, 10]. The anisotropic magnetoresistance [11] and anomalous Hall effect [1] are examples of nonlinear mechanisms which convert the oscillations of magnetic moments into a d.c. voltage. The use of a high mobility two-dimensional electron system (2DES) as a photodetector of stray magnetic fields [8, 12–17] creates new opportunities for probing localized spin resonances contactlessly, in magnetic volumes smaller than the wavelength of light [5, 6, 18, 19] with sensitivity comparable to superconducting detection [20, 21]. The mechanism by which near-field magnetic oscillations induce an electromotive force however remains unclear. Firstly, a 2D photodetector experiences zero net magnetic flux when a ferromagnet is placed in its proximity. This a priori suggests that any electromotive force is local. Secondly most physical quantities including magnetization and currents vanish under time averaging.

Here, we investigate the dipolar interactions of magnetic moments oscillating at microwave frequencies with a 2DES. We demonstrate that inductive coupling produces a long range electromotive force (*emf*) in the 2DES. We experimentally observe this *emf* in a modulation doped GaAs/$Al_{.33}$GaAs quantum well and use it to measure the spin wave eigenmodes of a single cobalt bar or disk of sub-100nm size. The photovoltage originates from the breaking of rotational symmetry by the magnetization whose vector components oscillate at different frequencies in the directions parallel and perpendicular to the Larmor magnetic field. The *emf* is found to be proportional to $\langle M_\mu \dot{M}_\nu - M_\nu \dot{M}_\mu \rangle$, $\{\mu,\nu\} \equiv \{x,y,z\}$ which does not cancel under time averaging as magnetization components M_x, M_y and M_z oscillate at different frequencies of precession, nutation [22] or ensemble-average Rabi cycling [23]. These frequencies are mixed and rectified by the Hall effect. We obtain a theoretical expression for the *emf* in the form of a Hall rectified Lenz law. The surface integral of the magnetic flux gives the strength of dipolar interaction. Ballistic Hall photo-voltammetry has a high detection sensitivity of 380 spins/$\sqrt{Hz}$ which arises from the *emf* being proportional to the very high mobility of 2D electrons. Electrically detected spin resonance spectra are compared to micromagnetic simulations.

We synthesized hybrid structures consisting of a single cobalt nanomagnet at the centre of a semiconductor Hall bar (Fig.1(a)). The heterojunction hosting the 2DES was set 30nm below the surface. The nanomagnets were fabricated through a combination of precision electron beam lithography and lift-off of a 30nm cobalt film deposited by magnetron sputtering. Preliminary quantum transport measurements gave electron mobility $\mu = 1.3 \times 10^6 \mathrm{cm}^2.\mathrm{V}^{-1}.\mathrm{s}^{-1}$ (4.2K) and areal electron density $n_s = 1.6 \times 10^{11} \mathrm{cm}^{-2}$. The applied magnetic field, B_a, was then rotated in the plane of the 2DES so that the only perpendicular magnetic field was the normal component of the fringing field. B_a was used to magnetize the bar magnet in the $x-y$ plane. B_a and the local demagnetizing field set the precession frequency of magnetic moments. We studied magnetic resonance over the $36-118$GHz bandwidth using 3 backward wave oscillators covering the Q, V and W bands. An over-moded circular waveguide terminated by a linear polarizer was used to guide microwaves to the sample space of a superconducting magnet. The polarizer aligned the microwave magnetic field parallel to the long axis of the nanomagnet (Fig.1(a)). The amplitude of the microwave magnetic field on the sample surface was $b \approx 10^{-5}$T as deduced from the 0.5mW microwave power output by the source through a 5.7mm×2.9mm waveguide section. Attenuation was -3dB and power losses were negligible. Microwave power was modulated at 830Hz. We measured the *emf* induced across a 8μm length of 2DES encompassing the nanomagnet (Fig.1(a)). Measurements were taken at 1.3K using lock-in detection.

The principle of ballistic Hall photo-voltammetry is schematically described in Fig.1(a). The fringing field of the bar magnet modulates the 2DES with spatially varying magnetic field $B_m(x)$ (Fig.1(b), black line). Time dependent oscillations of the magnetization induce eddy

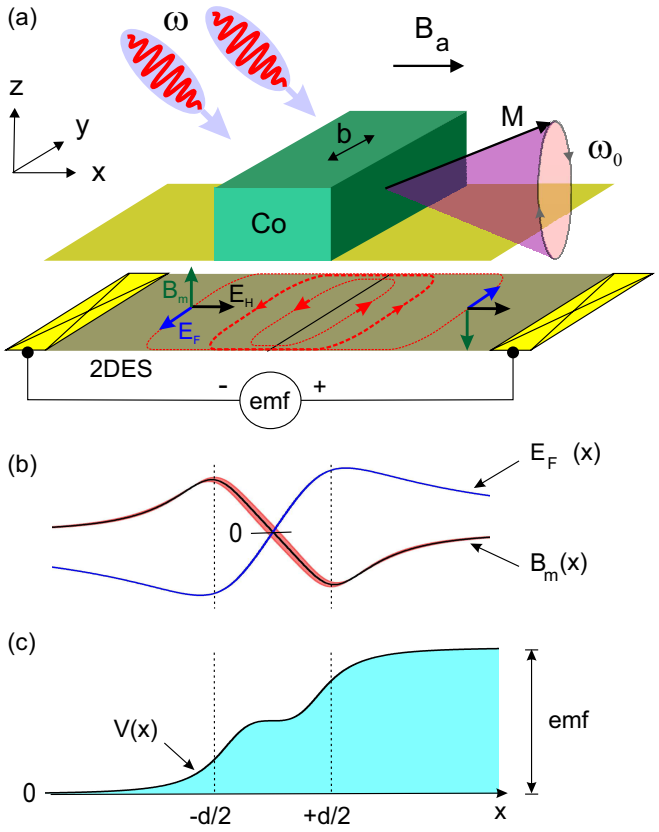

FIG. 1. *(color online)* **Principle of ballistic Hall photovoltammetry**. (a) A micromagnet (Co) modulates a 2DES with stray magnetic field $B_m(x)$. External magnetic field B_a magnetizes the bar magnet in the plane of the 2DES - either along the short or the long axis. Microwaves (ω, b) drive oscillations of the magnetization M, and subsequently of the magnetic modulation B_m and of the induction electric field E_F. Eddy current loops form in the 2DES (red dashed line). These currents are deflected by the Hall effect through electric field $E_H \propto \langle E_F\, B_m \rangle$ which gives a longitudinal *emf*. (b) Spatial variation of $B_m(x)$ and $E_F(x)$. (c) Spatial variation of the photovoltage $V(x) = -\int d\chi E_H(\chi)$ across the magnetically modulated 2DES. *Device dimensions*: magnet height $h = 30$nm, width $d = 100$nm, depth of 2DES $z_0 = 30$nm. ω_0 is the angular frequency of Larmor precession.

current loops in the 2DES (Fig.1(a)) which are driven by the rate of change of the magnetic modulation $\dot{B}_m$. Note that both the magnetic modulation $B_m(x)$ and the induction electric field $E_F(x)$ have asymmetrical profiles with respect to the centre of the bar (Fig.1(b)). Hence, the modulation field deflects eddy currents in the same direction on both sides of the magnet. The resulting Hall electric field, $E_H(x) \propto E_F(x) \times B_m(x)$, is symmetrical and generates a finite photovoltage $V(x) = -\int d\chi E_H(\chi)$ across the magnetic element (Fig.1(c)). The temporal oscillations of the photovoltage are rectified during magnetic resonance. At resonance, both B_m and E_F become a superposition of signals of different frequencies. For example, the dipolar magnetic field includes a contribution

$\sigma_\parallel$	$\sigma_\perp$	ι_x	ι_y
$\left\langle \frac{\mu}{1+\mu^2 B_m^2} \right\rangle$	0	$-\left\langle \frac{\mu^2}{1+\mu^2 B_m^2} B_m\, E_F \right\rangle$	0

TABLE I. Local time averaged conductivities and currents.

from magnetic poles perpendicular to B_a which oscillate at the Rabi frequency $\Omega = \mu_B b/\hbar$ and from magnetic poles parallel to B_a which oscillate at the Larmor frequency ω_0 where μ_B is the Bohr magneton. The resulting Hall electric field is an aperiodic signal with side bands $\omega_0 \pm \Omega$. The mean value of the photovoltage is therefore finite. In addition, because the amplitude of eddy currents increases with frequency, the photovoltage induced by the eddy current component oscillating at frequency ω_0 does not cancel out the photovoltage induced by eddy currents oscillating at frequency Ω.

We calculate the *emf* of a 2DES with a single occupied subband. At low magnetic field ($\mu B_m < 1$), the conductivity is weakly affected by radiation [24, 25] hence is:

$$\sigma(x,t) = \frac{n_s e\mu}{1+\mu^2 B_m^2} \begin{pmatrix} 1 & \mu B_m \\ -\mu B_m & 1 \end{pmatrix}, \qquad (1)$$

where μ depends on B_m through quantum corrections to the conductivity (supplemental material [26]). μ implicitly depends on x and t through its dependency on B_m. Ohm's law gives the instantaneous current density $\boldsymbol{J}(x,t) = \boldsymbol{\sigma}(x,t)\boldsymbol{E}(x,t)$ where the electric field $\boldsymbol{E}(x,t)$ incorporates the three following contributions: (i) the microwave electric field, $\boldsymbol{e}(t) = e\cos(\omega t)\,\boldsymbol{e}_x$, (ii) the electric field of Faraday induction, $\boldsymbol{E}_F(x,t)$ due to the rate of change of the modulation field, $\partial \boldsymbol{B}_m/\partial t = -\boldsymbol{\nabla} \wedge \boldsymbol{E}_F$ and, (iii) the Hall rectified electric field, $\boldsymbol{E}_H(x)$.

As no current is injected in the Hall bar, the requirement that $\langle \boldsymbol{J}(x,t) \rangle = 0$ gives the longitudinal and transverse components of $\boldsymbol{E}_H$ as solutions of:

$$\begin{cases} \sigma_\parallel(x) E_{H,x}(x) + \sigma_\perp(x) E_{H,y}(x) = \iota_x(x) \\ -\sigma_\perp(x) E_{H,x}(x) + \sigma_\parallel(x) E_{H,y}(x) = \iota_y(x) \end{cases}, \qquad (2)$$

where $\sigma_\parallel(x)$, $\sigma_\perp(x)$ are the time averaged conductivities and $\iota_x(x)$, $\iota_y(x)$ the time averaged current densities. These local coefficients are calculated in Table.I. The non-diagonal conductivity $\sigma_\perp$ and the transverse current ι_y vanish by time averaging. In addition, the spatial dependence of ι_y is the same as that of the flux of the magnetic modulation hence ι_y also cancels by integration over space. From Eq.2, the Hall electric field only has a longitudinal component $E_H(x) = \iota(x)/\sigma_\parallel(x)$ (Fig.1(a)).

In order to capture the essential physics while keeping the derivation analytical, our model considers the magnetization $\boldsymbol{M}$ to be the average density of magnetic moments. This average incorporates the spin waves formed

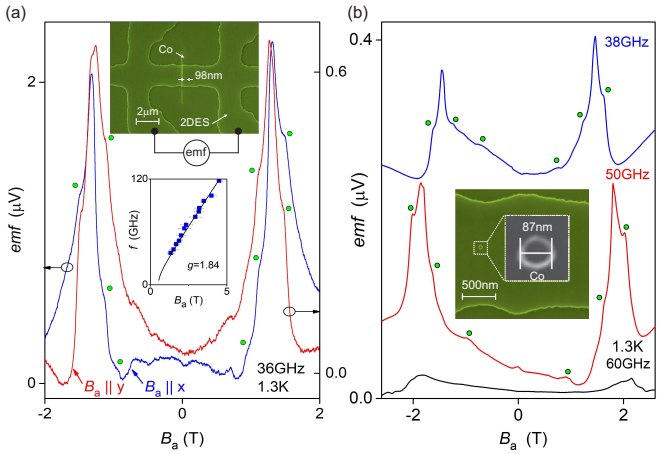

FIG. 2. *(color online)* **Photo-voltammetry of individual sub-100nm magnets** (a) Magnetic resonance spectrum of a cobalt bar magnet magnetized along its short axis (blue line) and long axis (red line) at 36GHz. The volume resonance of magnetic moments gives the main peak. Kinks in photovoltage spectrum (dot symbols) arise from spin excitations localized at the edges of the bar. *Top inset*: cobalt bar magnet of cross-section $d \times h = 98\text{nm} \times 30\text{nm}$ fabricated at the surface of a 2μm wide GaAs/AlGaAs Hall bar. *Lower inset*: frequency dispersion of the main resonance for $B_a \parallel x$ (square symbols) and predicted (full line). (b) Resonance spectrum of a cobalt disk at 38, 50 and 60GHz. *Inset*: cobalt disk of diameter $\varnothing = 87\text{nm}$ and height $h = 30\text{nm}$ on a Hall bar.

at the edges and in the bulk of the magnet which we calculate in detail below. With this approximation, the electric field of Faraday induction is transverse and equal to:

$$E_F(x,t) = -\int_{-\infty}^{x} d\xi\, \mu_0 \left[\alpha_x(\xi)\dot{M}_x(t) + \alpha_z(\xi)\dot{M}_z(t)\right], \tag{3}$$

and the stray magnetic field is:

$$B_m(x,t) = \alpha_x(x)\mu_0 M_x(t) + \alpha_z(x)\mu_0 M_z(t), \tag{4}$$

whose spatial variation is given by form factors [14]:

$$\begin{aligned} \alpha_x(x) &= -\frac{1}{2\pi}\left[g_0^+(x) - g_0^-(x) - g_h^+(x) + g_h^-(x)\right] \\ \alpha_z(x) &= -\frac{1}{2\pi}\left[f_0^+(x) - f_0^-(x) - f_h^+(x) + f_h^-(x)\right] \end{aligned}, \tag{5}$$

where $f_z^{\pm}(x) = \arctan\frac{x \pm d/2}{z_0 + z}$ and $g_z^{\pm}(x) = \ln\sqrt{(z_0+z)^2 + (x \pm d/2)^2}$. d and h are the width and height of the bar magnet and z_0 is the depth of the 2DES (Fig.1(a)). Eqs.3-5 are exact solutions of Maxwell's equations in both the far-field and near-field. Inserting $E_F(x,t)$ (Eq.3) and $B_m(x,t)$ (Eq.5) into $\iota_x(x)$ (Table.I), one obtains the Hall rectified electric field $E_H(x)$. The spatial variation of the photovoltage $V(x)$ generated by the Hall electric field follows from space integration as:

$$\begin{aligned} V(x) = &\frac{1}{\sigma_\parallel}\left\langle \frac{\mu^2\mu_0^2\, M_x(t)\dot{M}_z(t)}{1+\mu^2 B_m^2}\right\rangle A_{xz}(x) \\ &+ \frac{1}{\sigma_\parallel}\left\langle \frac{\mu^2\mu_0^2\, M_z(t)\dot{M}_x(t)}{1+\mu^2 B_m^2}\right\rangle A_{zx}(x). \end{aligned} \tag{6}$$

The dipolar field emanating from magnetic pole M_z threads the following area of 2DES:

$$A_{xz}(x) = \int_{-\infty}^{x} d\xi \int_{-\infty}^{\xi} d\zeta\; \alpha_x(\xi)\alpha_z(\zeta), \tag{7}$$

The dual area $A_{zx}(x)$, obtained by permutation of indices, is threaded with field emanating from pole M_x. We have used Eq.6 to plot the profile of the photovoltage in Fig.1(c). The *emf* is obtained by calculating $V(x)$ in the far field ($x \to +\infty$). The effective areas obey the sum rule $A_{xz}(+\infty) + A_{zx}(+\infty) = 0$. As long as the magnetic modulation is not too large ($\mu B_m < 1$), the *emf* takes the simple form:

$$emf = \mu\mu_0^2 A \left\langle M_z\dot{M}_x - M_x\dot{M}_z\right\rangle. \tag{8}$$

This is effectively a Hall rectified Lenz law. The *emf* is proportional to the rate of change of the magnetic flux created by resonating magnetic moments $\dot{M}_x$ (resp. $\dot{M}_z$). The time averaged term in Eq.8 cancels off-resonance when M_x and M_z oscillate at the same frequency. However when the system crosses resonance, $\dot{M}_z = \omega_0 M_z$ and $\dot{M}_x = \Omega M_x$ giving a finite *emf*. The *emf* is proportional to the strength of dipolar coupling between the magnet and the 2DES through area $A \equiv A_{zx}(+\infty)$ which depends on magnet dimensions and separation from the 2DES. The *emf* is also proportional to the electron mobility, μ, which can be as high as $36 \times 10^6 \text{cm}^2.\text{V}^{-1}.\text{s}^{-1}$ [27, 28] and critically grants exceptional sensitivity to the detection of spin resonance.

Figs.2(a) and (b) show the magnetic resonance spectra which we obtained by measuring the *emf* across a single cobalt bar magnet and a sub-100nm disk respectively. The position of the main resonance follows the frequency dispersion predicted by Kittel's equation for the bar when shape anisotropy dominates over magnetocrystalline anisotropy ($B_a \parallel x$) [26]. When $B_a \parallel y$, the reverse occurs and although the resonance does shift to lower magnetic field, this shift is smaller than that anticipated from shape anisotropy alone. For example at 36GHz (Fig.2(a)), the peak shifts from 1.35T ($B_a \parallel x$) to 1.15T ($B_a \parallel y$) instead of the predicted 0.55T due to magnetocrystalline anisotropy pinning the resonance position at 1.05T [26]. The *emf* spectra of both Co bar

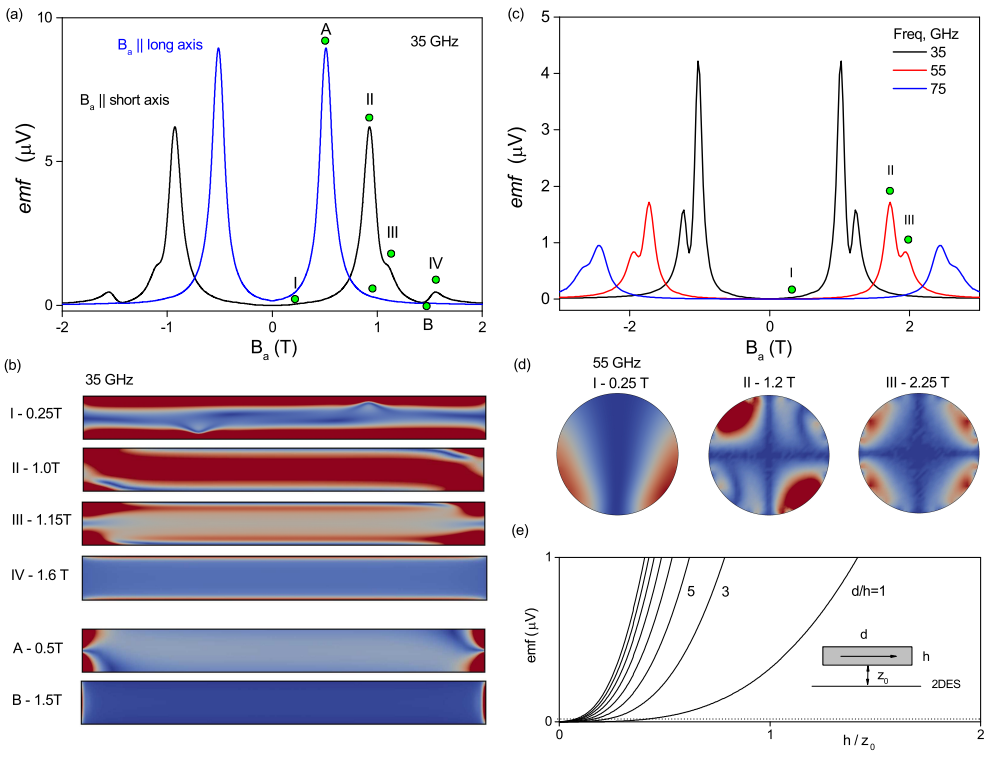

FIG. 3. *(color online)* **Theoretical photo-voltammetry spectra** (a) *emf* spectrum of a cobalt bar magnet of cross-section $d \times h = 80\text{nm} \times 30\text{nm}$ when the magnetization is either along the short axis (black line) or the long axis (blue line). (b) Maps of the local amplitudes of magnetic moment oscillations corresponding to the *emf* peaks I-IV and A-B. (c) *emf* spectrum of a cobalt disk of diameter $\varnothing = 80\text{nm}$ and height $h = 30\text{nm}$. (d) Spin wave eigenmodes corresponding to the *emf* peaks I-III. (e) Dependence of the *emf* on the dimensions of a bar magnet of constant cross-section. *Parameters*: cobalt saturation magnetization, $\mu_0 M_s = 1.8\text{T}$; Gilbert damping, $\alpha = 0.05$; exchange interaction constant, $A = 30 \times 10^{-12}$ J/m.

and disk (Fig.2(b)) show a fine structure superimposed on the main peak (circle symbols) which follows the same frequency dispersion as the main peak [26]. The small amplitude of kinks suggests low-dimensional spin waves quantized by the inhomogeneous dipolar field near the poles [5, 6, 29]. The ability to inductively detect these local resonances, which involve of a few hundred thousand Bohr magnetons, relies on the long-lived eddy currents of ballistic electrons. This implies magnet sizes smaller than the electron mean free path, and Hall bars narrower than the mean free path to minimize thermalization of eddy currents between the Co disk and Hall bar edges.

In order to test our theory, we performed micromagnetic calculations of the *emf* for both magnet geometries. These calculations are intended to predict qualitative features of the resonant peaks rather than the exact peak positions as magnetocrystalline anisotropy of polycrystalline cobalt and interfacial magnetoelastic effects were not included [26]. We computed the magnetization as a time series using mumax^3 [30] and inserted this in Eq.8 to obtain the *emf*. The magnetic volume was partitioned into 5nm×5nm cells for the bar and 2nm×2nm cells for the disk, to resolve the dipolar-exchange spin waves localized at the edges. The magnetic field B_a was varied in the range $-4\text{T} \rightarrow +4\text{T}$ in steps of 25mT. During each step, a microwave magnetic field $b = 10^{-5}\text{T}$ was applied and the time dependence of the magnetization was calculated [26]. The instantaneous magnetization was obtained by averaging the magnetic moments in each cell. The $M_x(t)$ and $M_z(t)$ time series data were inserted in Eq.8 to calculate the *emf* and its dependence on B_a. Time averaging was weighted by probability $e^{-t/\tau}$ that Hall voltage oscillations remain coherent at time t. The damping rate $\tau^{-1} = \tau_\gamma^{-1} + \tau_\mu^{-1}$ compounded the Gilbert damping time of the magnetization, $\tau_\gamma = (\alpha\gamma M_s)^{-1} \approx 63$ ps, with the decay time of eddy currents $\tau_\mu = m^*\mu/e \approx 48$ps. $\alpha = 0.05$ is Gilbert's damping (Co), γ is the gyromagnetic ratio, e and m^* are the electron charge and effective mass respectively.

The calculated *emf* spectra are shown in Fig.3. Resonance in the bulk of the bar magnet (Fig.3(a)) gives a resonance peak (peak A) which shifts from 0.5T to

0.95T (peak II) as the magnetization rotates from the long axis to the short axis. The theoretical spectra exhibit a series of satellite peaks (I-III-IV) as in experiments. These peaks correspond to spin wave eigenmodes confined near the poles by wells of demagnetizing field (Fig.3(b)) [6, 29]. These modes are increasingly localized as B_a increases [5]. A distinguishing feature of the cobalt disk (Fig.3(c)) is the subsidiary peak (peak III) after the main resonance (peak II), also observed in experiments. Simulations ascribe peaks II and III to the dipolar and quadrupolar spin wave eigenmodes plotted in Fig.3(d).

Fig.3(e) shows the dependence of the *emf* on the strength of dipolar coupling between the magnet and the 2DES as a function of h/z_0 for bar magnets of different aspect ratios d/h. Smaller 2DES-magnet separations or thicker magnets increase the *emf*. For our disk of dimensions $h = z_0$ =30nm and radius=43nm, we estimate the detection sensitivity to be 380spins/$\sqrt{Hz}$ [26]. This sensitivity is comparable to that of quantum circuits at mK temperatures, 65spins /$\sqrt{Hz}$ [20, 21], while our detection method retains the versatility of less sensitive induction methods, $\approx 10^{10}$ spins /$\sqrt{Hz}$ [31]. Other techniques such as the photo-ionization of nitrogen vacancies in diamond [32] or Coulomb blockaded quantum dots [33–35] achieve greater spin detection sensitivities but are less versatile. The *emf* detected with the present technique varies as a square root of microwave power as expected from Eq.8 [26]. This is in contrast to the power dependence of spin rectification by anisotropic magnetoresistance effects which is linear [1].

We have observed magnetic resonance in the photovoltage at temperatures between 1.3K and 85K [26]. Photodetected spin resonance may be observed at even higher temperatures using non polar 2D materials, such as graphene, which have high mobility at room temperature [28]. In summary, ballistic Hall photo-voltammetry is a non-invasive and sensitive probe which has significant advantages for studying local spin dynamics.

This research was supported by the European Union FP7 IRSES 318973.

* A.R.Nogaret@bath.ac.uk

[1] M. Harder, Y. Gui, and C. M. Hu, Phys.Rep. **661**, 1 (2016).

[2] Y. S. Gui, S. Holland, N. Mecking, and C. M. Hu, Phys.Rev.Lett. **95**, 056807 (2005).

[3] S. T. B. Goennenwein, S. W. Schink, A. Brandlmaier, A. Boger, M. Opel, R. Gross, R. S. Keizer, T. M. Klapwijk, A. Gupta, H. Huebl, C. Bihler, and M. S. Brandt, Appl. Phys. Lett. **90**, 162507 (2007).

[4] A. A. Awad, G. R. Aranda, D. Dieleman, K. Y. Guslienko, G. N. Nakazei, B. A. Ivanov, and F. G. Aliev, Appl. Phys. Lett. **97**, 132501 (2010).

[5] J. P. Park, P. Eames, D. M. Engebretson, J. Berezovsky, and P. A. Crowell, Phys.Rev.Lett. **89**, 277201 (2002).

[6] J. Jorzick, S. O. Demokritov, and B. Hillebrands, Phys.Rev.Lett. **88**, 047204 (2002).

[7] S. Jain, V. Novosad, F. Y. Fradin, J. E. Pearson, V. Tiberkevich, A. N. Slavin, and S. D. Bader, Nature Comm. **3**, 1330 (2012).

[8] P. Saraiva, A. Nogaret, J. C. Portal, H. E. Beere, and D. A. Ritchie, Phys.Rev.B **82**, 224417 (2010).

[9] A. V. Chumak, A. A. Serga, and B. Hillebrands, Nature Comm. **5**, 4700 (2014).

[10] K. Vogt, F. Y. Fradin, J. E. Pearson, T. Sebastian, S. D. Bader, B. Hillebrands, A. Hoffmann, and H. Schultheiss, Nature Comm. **5**, 3727 (2014).

[11] H. Zhou, X. Fan, F. Wang, C. Jiang, J. Rao, X. Zhao, Y. S. Gui, C. M. Hu, and D. Xue, Appl. Phys. Lett. **104**, 102401 (2014).

[12] A. K. Geim, S. V. Dubonos, J. G. S. Lok, I. V. Grigorieva, J. C. Maan, L. Theil Hansen, and P. E. Lindelof, Appl. Phys. Lett. **71**, 2379 (1997).

[13] D. N. Lawton, A. Nogaret, S. J. Bending, D. K. Maude, J. C. Portal, and M. Henini, Phys.Rev.B **64**, 033312 (2001).

[14] A. Nogaret, J.Phys.Cond.Mat. **22**, 253201 (2010).

[15] D. Uzur, A. Nogaret, H. E. Beere, D. A. Ritchie, C. H. Marrows, and B. J. Hickey, Phys.Rev.B **69**, 241301 (2004).

[16] A. Nogaret, D. N. Lawton, D. K. Maude, J. Portal, and M. Henini, Phys.Rev.B **67**, 165317 (2003).

[17] A. Nogaret, P. Mondal, A. Kumar, S. Ghosh, H. Beere, and D. Ritchie, Phys.Rev.B **96**, 081302 (2017).

[18] G. Gubbiotti, S. Tacchi, G. Carlotti, N. Singh, S. Goolaup, A. O. Adeyeye, and M. Kostylev, Appl. Phys. Lett. **90**, 092503 (2007).

[19] U. Ebels, J. L. Duvail, P. E. Wigen, L. Piraux, L. D. Buda, and O. K., Phys.Rev.B **64**, 144421 (2001).

[20] A. Bienfait, J. J. Pla, Y. Kubo, M. Stern, X. Zhou, C. C. Lo, C. D. Weis, T. Schenkel, M. L. W. Thewaldt, D. Vion, D. Esteve, B. Julsgaard, K. Mølmer, J. J. L. Morton, and P. Bertet, Nature Nanotech. **11**, 253 (2016).

[21] S. Probst, A. Bienfait, P. Campagne-Ibarcq, J. J. Pla, B. Albanese, J. F. Da Silva Barbosa, T. Schenkel, D. Vion, D. Esteve, K. Mølmer, J. J. L. Morton, R. Heeres, and P. Bertet, Appl.Phys.Lett. **111**, 202604 (2017).

[22] D. Böttcher and J. Henk, Phys.Rev.B **86**, 020404 (2012).

[23] A. Capua, C. Rettner, S. H. Yang, T. Phung, and S. P. Parkin, Nature Comm. **8**, 16004 (2017).

[24] I. A. Dmitriev, M. G. Vavilov, I. L. Aleiner, A. D. Mirlin, and D. G. Polyakov, Phys.Rev.B **71**, 115316 (2005).

[25] A. Nogaret, F. Nasirpouri, J. C. Portal, H. E. Beere, D. A. Ritchie, A. T. Hindmarch, and C. H. Marrows, EPL **94**, 28001 (2011).

[26] (2021), see Supplemental Material at [URL inserted by publisher] for frequency dispersion data, anisotropy and spin sensitivity calculations.

[27] D. G. Schlom and L. N. Pfeiffer, Nature Mat. **9**, 881 (2010).

[28] J.-H. Chen, C. Jang, S. Xiao, M. Ishigami, and M. S. Fuhrer, Nature Nanotech. **3**, 206 (2008).

[29] C. Bayer, J. Jorzick, S. O. Demokritov, A. N. Slavin, K. Y. Guslienko, D. V. Berkov, N. L. Gorn, M. P. Kostylev, and B. Hillebrands, in *Spin Dynamics in confined Magnetic Structures III*, edited by B. Hillebrands and A. Thiaville (Springer-Verlag, Berlin, Heidelberg, 2006) Chap. 2, pp. 57–103.

[30] A. Vansteenkiste, J. Leliaert, M. Dvornik, M. Helsen, F. Garcia-Sanchez, and B. Van Waeyenberge, AIP Advances **4**, 107133 (2014).
[31] Y. Twig, E. Suhovoy, and A. Blank, Rev.Sci.Instr. **81**, 104703 (2010).
[32] F. M. Hrubesch, G. Braunbeck, M. Stutzmann, F. Reinhard, and M. S. Brandt, Phys.Rev.Lett. **118**, 037601 (2017).
[33] A. Morello, J. J. Pla, F. A. Zwanenburg, K. W. Chan, K. Y. Tan, H. Huebl, M. Mottonen, C. D. Nugroho, C. Yang, J. A. van Donkelaar, A. D. C. Alves, D. N. Jamieson, C. C. Escott, L. C. L. Hollenberg, R. G. Clark, and A. S. Dzurak, Nature **467**, 687 (2010).
[34] J. M. Elzerman, R. Hanson, L. H. Willems van Beveren, B. Witkamp, L. M. K. Vandersypen, and L. P. Kouwenhoven, Nature **430**, 431 (2004).
[35] F. H. L. Koppens, B. C., K. J. Tielrooij, I. T. Vink, K. C. Nowack, T. Meunier, L. P. Kouwenhoven, and L. M. K. Vandersypen, Nature **442**, 766 (2006).